Journal of Thermal Analysis and Calorimetry, Vol. 93 (2008) 3, 1013–1019

NUMERICAL MODEL OF A LARGE-SCALE OXYGEN CONSUMPTION FIRE CALORIMETER

S. C. Kim[1*] *and M. Bundy*[2]

[1]School of Fire and Disaster Prevention, Kyungil University, Kyungbuk 712-701, Korea
[2]Building and Fire Research Lab., NIST, Gaithersburg, Maryland 20899, USA

The present study introduces a volumetric heat and mass source model to investigate the flow field inside the hood and duct system and optimize the sampling technique in a large scale fire calorimeter. The model was validated using experimental measurements of the oxygen depletion factor, gas temperature and heat release rate. The calculated heat release rates determined using the CFD model were in good agreement with the experiments with the maximum discrepancy between the simulations and experiments being less than 5%. A series of CFD simulations were performed to examine the effects of sampling location, and the number of sampling points on the uncertainty of the heat release calculation. Detailed flow characteristics were analyzed to understand the complicated internal duct flow.

Keywords: *calorimeter, calorimeter design, CFD, fire, fire model, oxygen consumption*

Introduction

The heat release rate (HRR), which describes the fire size of burning materials, is a fundamental parameter that is essential to estimate fire hazards and design fire protection systems [1–3]. Among the various measurement methods for determining the heat release rate, oxygen consumption calorimetry is the most common. The oxygen consumption principle is based on the assumption that the amount of heat released per unit mass of consumed oxygen is approximately constant for most common burning materials containing C, H and O [4]. Thus, the heat release rate can be approximated by measuring the oxygen deficit in the exhaust gas flow. The key parameters needed to determine heat release rate are the entrained air mass flow and the oxygen depletion. These values are typically determined from real time measurements of velocity, temperature and species concentration in the exhaust duct flow. The heat release rate calculation uses representative values of measured quantities at the sampling position in the exhaust duct. The exhaust duct flow profile is essential to the accuracy of the oxygen consumption calorimetry measurement. In a large exhaust hood, however, it is sometimes impractical to have a sufficiently long straight duct to obtain fully developed flow due to the spatial restrictions of the test facility. Therefore, the optimal design of a duct system including the hood and the determination of sampling position is essential to reduce the measurement uncertainty. Many previous designs of hood and duct systems have relied on engineering intuition or simple exhaust flow calculations to examine the duct flow characteristics and design optimization. In the present study, a simplified fire source model based on a volumetric heat and mass source term was used to examine the detailed flow characteristics in the exhaust duct. The effects of the geometrical configuration, sampling position and number of the sampling points of measured quantities on the heat release rate calculation were also investigated.

Experimental

HRR measurements based on the oxygen consumption calorimetry were conducted using the newly installed 1 MW prototype calorimeter (3 m×3 m hood) at the NIST Large Fire Research Laboratory. Although this calorimeter has a maximum capacity of 1 MW, it is typically used for fires less than 500 kW to prevent flames from entering the duct. This instrument is primarily used for studying the evolution of fires on single burning items, such as upholstered furniture. A detailed description of the measurement method can be found in a report on the performance of the 3 MW calorimeter (6 m×6 m hood) [5]. The measurement of exhaust flow velocity and gas volume fractions were used to determine the HRR based on the formulation derived by Parker [6]. The exhaust flow rate and extractive gas measurements were performed in a horizontal section of the 0.48 m diameter steel duct. A bi-directional probe [7] located 0.09 m from the top

* Author for correspondence: sungkim.phd@gmail.com

1388–6150/$20.00

Akadémiai Kiadó, Budapest, Hungary
Springer, Dordrecht, The Netherlands

edge of the duct was used to measure the exhaust flow velocity. The exhaust gas was sampled through a perforated tube positioned vertically across the duct downstream of the velocity probe. The calorimeter is shown schematically in Fig. 1. The combined expanded (95% confidence level) relative uncertainty of the HRR measurements reported here was less than 11%, based on a propagation of uncertainty analysis. The exhaust mass flow rate was the largest component of uncertainty in the HRR measurement. The heat source for the experiments was a well controlled natural gas fire. The natural gas composition, heating value, temperature, pressure and volumetric flow rate were directly measured to determine the reference fire's heat release rate with a combined expanded relative uncertainty of 2.5%.

Numerical models

Fire source model – volumetric heat and mass source concept

Volumetric heat source models have been widely used in a number of studies to simplify the simulation of complex burning phenomena [8–10]. The fire source is directly modeled with a given heat release rate as an energy source term per unit volume. This type of model has been mainly used to predict the thermal flow field in a fire compartment, but it has some limitations providing information about the species field which requires a detailed chemical model of the combustion process. In order to apply the model to a fire source in the CFD simulation for oxygen consumption calorimetry, an additional mass source term should be considered. As seen in Fig. 1, the volumetric heat and mass source model assumes that the oxygen in the entrained air is consumed and combustion products and thermal energy are released from the fire source. All of the quantities are assumed to be uniformly distributed in the fire source and complete combustion is assumed for hydrocarbon fuels:

$$\nu_f C_x H_y + \nu_{O_2} O_2 \rightarrow \nu_{CO_2} CO_2 + \nu_{H_2O} H_2O \qquad (1)$$

The fuel mass burning rate, $\dot{m}_f$, is determined by the ratio of the prescribed heat release rate, Q and the heat of combustion of the fuel, $\Delta H_{C,f}$.

$$\dot{m}_f = \frac{Q}{\Delta H_{C,f}} \qquad (2)$$

The energy source term per unit volume of fire source is determined by the given heat release rate and the volume of fire source.

$$\dot{q}''' = \frac{Q}{V_f} \qquad (3)$$

$$V_f = A_f h_f \qquad (4)$$

where, $\dot{q}'''$ is the heat generation rate per unit volume of fire source and V_f, A_f and h_f represent the geometric fire source volume, area and height, respectively. The mass production (or consumption) rate of each species per unit volume of the fire source ($\dot{m}'''$) is calculated as follows:

$$\dot{m}''' = \frac{\dot{m}_f}{V_f}\left(\frac{\nu_i MW_i}{\nu_f MW_f}\right) \qquad (5)$$

where ν represents the stoichiometric coefficients and the subscripts *f* and *i* denote the fuel and each species. The heat generation and mass production of CO_2 and H_2O are considered as source terms in the energy and species conservation equations, respectively. The mass consumption of the oxygen is treated as a sink term in the species conservation equation for O_2. The present study considered methane fires with given heat release rates of 100, 200 and 400 kW.

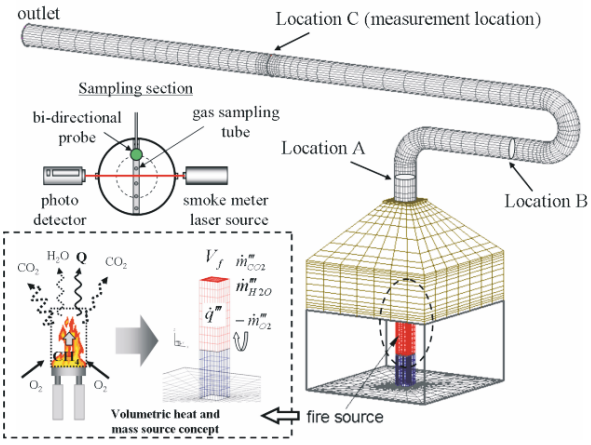

Fig. 1 Schematic of oxygen consumption calorimeter and concept of volumetric heat and mass source

Numerical solution

The computational grid, including exhaust duct and hood system, was divided into approximately 40000 cells of a hexahedral type mesh. The space under the hood was assumed to be exposed to ambient air. The flow fields were calculated using the commercially available CFD package FLUENT 6.0** to model the fire-driven flow. The k–ε turbulence model with buoyancy modification and the assumption of an incompressible ideal gas were applied to solve the

** Certain commercial products are identified to adequately describe the computational method. This is no way implies endorsement by NIST.

Reynolds stress term and density change, respectively. The measured temperature and humidity were directly applied as initial conditions for the calculation. Because water was trapped from the sampled gas, the measured O_2 and CO_2 volume fraction were converted into wet values for the CFD model.

$$X_{\mathrm{i,wet}} = (1 - X_{\mathrm{H_2O}}) X_{\mathrm{i,dry}} \tag{6}$$

where X_i represents the volume fraction of species *i*. The initial velocity and turbulent quantities were assumed to be zero in the exhaust duct. A pressure boundary condition at the end of the duct was applied to drive the exhaust flow. An extensive numerical study was performed to find the relationship between the measured velocity at the probe location and the prescribed pressure difference at the boundary. A thermally thin wall boundary condition was applied on the duct wall to account for heat losses from duct to ambient air.

HRR Calculation

The heat release rate can be calculated from the oxygen mass consumption rate as follows:

$$Q = \Delta H_{\mathrm{C,O_2}} (\dot{m}^{\circ}_{\mathrm{O_2}} - \dot{m}_{\mathrm{O_2}}) \tag{7}$$

where $\Delta H_{\mathrm{C,O_2}}$ denotes the heat of combustion per unit mass of oxygen and $\dot{m}^{\circ}_{\mathrm{O_2}}$ and $\dot{m}_{\mathrm{O_2}}$ are the oxygen mass flow rate in the incoming air and the oxygen mass flow rate in the exhaust duct, respectively. Because direct measurement of $\dot{m}^{\circ}_{\mathrm{O_2}}$ is not practical for an open system, the oxygen depletion factor (ϕ) is defined in terms of $\dot{m}^{\circ}_{\mathrm{O_2}}$ and $\dot{m}_{\mathrm{O_2}}$ which can be expressed in terms of the measured volume fraction of the gas species [6, 11].

$$\phi = \frac{\dot{m}^{\circ}_{\mathrm{O_2}} - \dot{m}_{\mathrm{O_2}}}{\dot{m}^{\circ}_{\mathrm{O_2}}} = \frac{X^{\circ}_{\mathrm{O_2}} (1 - X_{\mathrm{CO_2}} - X_{\mathrm{CO}}) - X_{\mathrm{O_2}} (1 - X^{\circ}_{\mathrm{O_2}})}{(1 - X_{\mathrm{O_2}} - X_{\mathrm{CO_2}} - X_{\mathrm{CO}}) X^{\circ}_{\mathrm{O_2}}} \tag{8}$$

where X_i represents the measured volume fraction of species *i* at the sampling positions and X°_{i} is the measured volume fraction of species *i* in the incoming air. The heat release rate can be calculated using the following simplified equation from the measured volume fractions, the mass flow rate in the exhaust duct, $\dot{m}_e$ and the chemical expansion factor, α [5, 6]:

$$Q_{\mathrm{m}} = \Delta H_{\mathrm{C,O_2}} \phi \frac{\dot{m}_{\mathrm{e}}}{1 + \phi(\alpha - 1)} (1 - X^{\circ}_{\mathrm{H_2O}}) X^{\circ}_{\mathrm{O_2}} \frac{MW_{\mathrm{O_2}}}{MW_{\mathrm{air}}} \tag{9}$$

where MW_i is the molecular mass of species *i*.

Results and discussion

Validation of the CFD model

Prior to the analysis of the flow characteristics of the oxygen consumption calorimeter, the results of the CFD model were compared to experimental measurements. Figure 2a compares the CFD model and experimental values of the oxygen depletion factor and the gas temperature at the sampling position. The error bars represents the magnitude of the fluctuation of the measurements. The results predicted by the CFD model were consistent with the measurements at the sampling position. The difference between experiments and CFD model in the oxygen depletion factor was less than 2% for the range of given heat release rates. However, the predicted gas temperature were quite different than the measured results, the maximum difference was about 40°C for the given heat release rate of 400 kW. Figure 2b compares the calculated heat release rates, using Eq. (9), to the measured results. Because the velocity at the sampling position was directly applied to calculate the exhaust mass flow rate, which did not include the flow shape factor, the

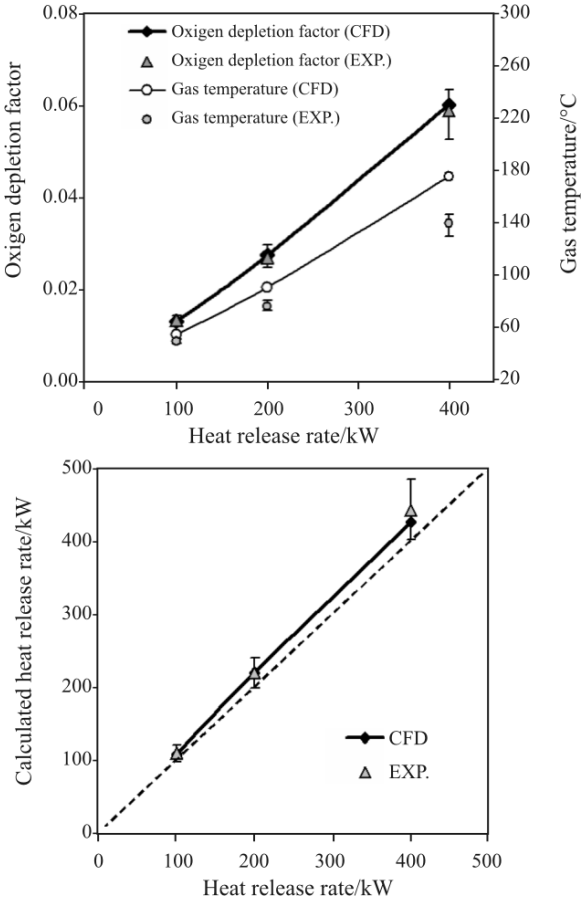

Fig. 2 Comparison of key parameters between the CFD model and measurements as a function of the given heat release rates

measurements and simulations over-predict the actual heat release rate. In practice, the shape factor is accounted for by using a calibration coefficient (sometimes called a C-factor). The calculated heat release rates using CFD agreed within experimental error with the measured results. The maximum discrepancy in the calculated heat release rate between the CFD simulation and experiment was approximately 4%, which can be considered as a reasonable value for CFD validation.

Examination of flow characteristics

The comparison of the CFD model with experiments enables further understanding of the flow field including the buoyant flow under the hood and the internal flow in the exhaust duct. Figure 3 shows the flow field at the center plane of the calorimeter for the case of nominal heat release rate of 200 kW. As shown in Fig. 3a, the fresh air was entrained from the ambient due to the forced exhaust flow and buoyant flow of the fire itself. The entrained ambient air was mixed with the combustion gases and the fire plume passes through the hood and into the entrance of the exhaust duct. This entrained mixing process plays a role in diluting the combustion products and cooling the sample gas inside the exhaust duct. At the corner of the hood, large vortices are predicted, due to the hood curtain which is used to prevent loss of combustion products from the hood. The converged flow at the entrance of the exhaust hood shows the highest velocity magnitude in the entire duct, higher than 20 m s^{-1} (Fig. 3b). From the volumetric heat and mass source model, the maximum temperature at the fire source is above 1700°C. But the gas temperature of the combustion mixture inside the duct is below 80°C except near the entrance of the duct. Figure 3 shows that the velocity at the upper part of the horizontal duct was relatively higher than that of the lower part, while the temperature field looks quite uniform across the duct.

Ideally, the use of a straight duct from the entrance of the hood is the best option to minimize the effect of the duct geometry on the flow structure. Actually, the curved ducts of 90 and 180° are typically used to minimize space requirements and construction and maintenance costs. Principally, the flow in the curved ducts differ from a straight duct through a

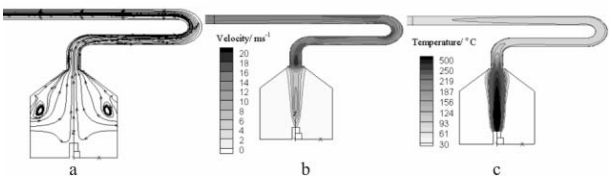

Fig. 3 Flow field for the case of the heat release rate of 200 kW; a – streamline, b – velocity, c – temperature

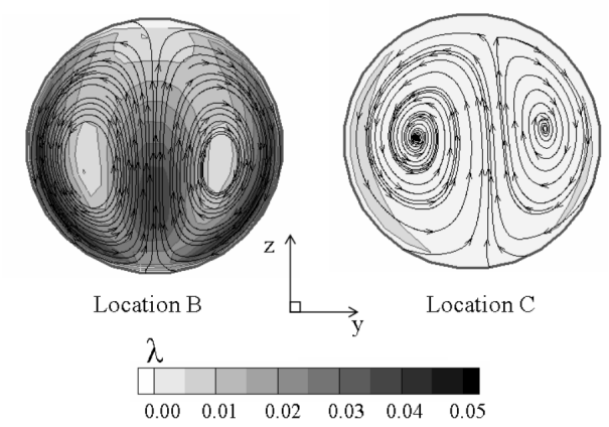

Fig. 4 Streamlines and lateral to axial velocity ratio, λ, field at two cross-sections of sampling position B and C for a 200 kW fire

secondary flow in the plane normal to the stream-wise flow. It is well known that centrifugal forces can cause a secondary flow in the plane normal to the primary axial flow in a curved duct [12, 13]. It has been reported that the secondary flow plays a role in enhancing transverse mixing, causing a higher heat transfer coefficient and reducing axial dispersion. Figure 4 shows the streamline at the sampling locations B and C. The sampling locations B and C are positioned 3 m downstream of the first 90° bend in the duct and 8 m downstream of the 180° bend in the duct, respectively. A pair of counter-rotating vortices, which is formed inside the curved ducts, is still observed at the sampling locations. In order to quantify the lateral velocity magnitude at the sampling location, the ratio between lateral and axial velocity (λ) is defined as follows:

$$\lambda = \frac{\sqrt{v^2 + w^2}}{|u|} \tag{10}$$

where u represents the axial velocity component and, v and w denote the lateral velocity components. The maximum value of the λ at the location B reached 8%, but was less than 1% at location C, farther downstream from the curved duct. Figure 5 compares the velocity and temperature profiles normalized by their maximum value at three difference locations as shown in Fig. 1. These profiles are important to calculate the mean quantities considering the flow shape. The pathlength from the entrance of the duct to locations of A, B and C along the centerline of the exhaust duct is 0.6, 4.2 and 14.4 m, respectively. As observed in Fig. 3, the temperature profiles are more uniform than the velocity profiles across the duct. Moreover, the temperature profile at location B is similar to that of location C, while the velocity profiles are quite different from each other. This similarity also exists in the species field, which is composed of passive

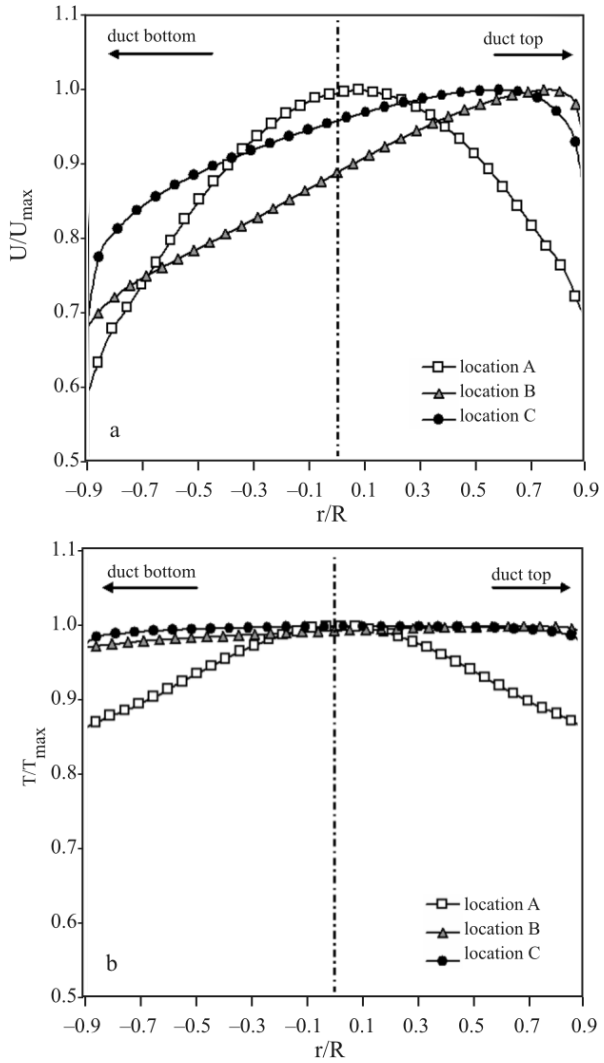

Fig. 5 Comparison of the a – velocity and b – temperature profiles at three different locations (A, B and C) in the exhaust duct for a 200 kW fire; a – velocity profiles, b – temperature profiles

scalar quantities. The results show that the flow field needs a longer entrance length than the thermal and mass fields to reach fully developed conditions. Among the measurement quantities needed to calculate the heat release rate such as the velocity, temperature and species, the determination of the mean velocity at the sampling section which is directly applied to calculate the exhaust mass flow rate is the largest contribution to the uncertainty of heat release rate measurement [5, 14]. The uncertainty of the mean velocity not only comes from uncertainty of probe itself, but also due to the flow shape factor which is used to convert between the actual measured velocity to the mean velocity across the sampling section. Experimentally, limitations exist on installing many probes to determine the velocity profile due to flow blockage and probe interaction effects. The present study examines the effect of number of measurement points on the mean velocity and the uncertainty of the heat release rate. Figure 6 shows the computed velocity profile with the measured instantaneous velocity at the probe location for a 200 kW fire. The time average of the measured instantaneous velocity at the bi-directional probe position is approximately 15.2 m s^{-1} with the mean fluctuation ($\overline{u}$') of 0.8 m s^{-1}. The results of the model show that the velocity probe is located near the maximum of the velocity profile. This value is quite different from the mean velocity across the duct. In the CFD calculation, the line averaging and the surface averaging velocity are calculated over the centerline of the sampling section and the sampling surface, respectively:

$$\overline{U_{\mathrm{H}}} = \frac{1}{H_{\mathrm{D}}}\int U \mathrm{d}h = \frac{1}{H_{\mathrm{D}}}\sum_{\mathrm{i}=1}^{\mathrm{N}} U_{\mathrm{i}}\, h_{\mathrm{i}} \qquad (11)$$

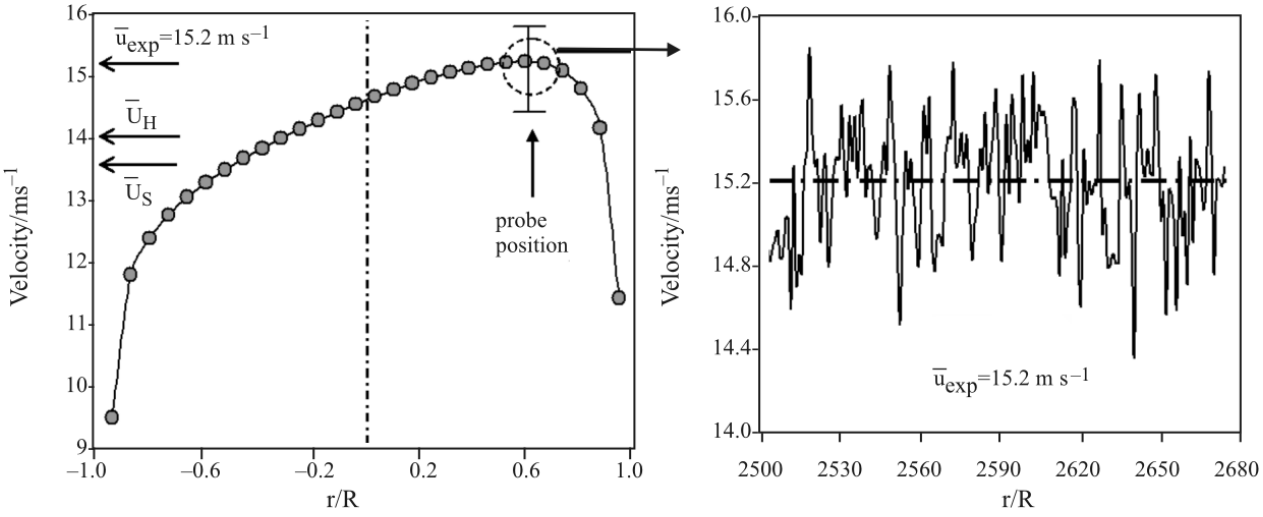

Fig. 6 The computed velocity profiles at the sampling section, location C and the measured instantaneous velocity using a bi-directional probe for 200 kW fire

$$\overline{U_S} = \frac{1}{A_D}\int U \mathrm{d}A = \frac{1}{A_D}\sum_{j=1}^{M} U_j A_j \qquad (12)$$

The relative error of heat release rate using the line averaged velocity compared to the surface averaged velocity is defined as follows:

$$\psi = \left(\frac{Q_H - Q_S}{Q_S} \right) \cdot 100 \qquad (13)$$

The calculated line averaged velocity and surface averaged velocity are 14.0 and 13.7 m s^{-1}, respectively. The calculated ψ, using the surface averaged and line averaged velocities, was less than 2.8 and 1%, respectively. The optimal number of the sampling positions required to resolve the velocity profile is important to determine an accurate effective velocity. To investigate the effect of the number of sampling points on the averaged velocity, the present study compared the averaged velocity for different numbers of sampling points. In this calculation, the effects of the probes on the flow field was assumed to be negligible. Figure 7a shows the representative velocity ($\overline{U}$), which is averaged over the number of sampling positions which were evenly located in the exhaust duct, normalized by the surface average velocity ($\overline{U}_s$). As expected, the representative velocity became closer to the surface average velocity as the number of sampling positions increased. But the gradient of the velocity ratio decreased with increasing the number of sampling positions. Figure 7b represents the relative percentage error of the heat release calculation (Eq. (13)) as function of the number of sampling positions for the different heat release rates. As may be expected, the ψ decreased as the number of sampling position increased. This is probably because increasing the number of sampling positions gives a more accurate representation of the velocity to calculate the exhaust mass flow rate. The ψ decreased about from 7.5 to 4%, while the mean velocity ratio ranged from 0.93 to 0.97. The ψ based on the average velocity for 6 sampling points was less than 5% for this size hood and duct system. Figure 8 shows the turbulent kinetic energy field in the hood and duct system for the case of nominal heat release rate of 200 kW. The magnitude of the turbulent kinetic energy was high at the entrance of the duct and curved duct because of the high mean shear due to the effect of the flow contraction, separation and pressure gradient. The high levels of turbulence generated in the curved duct quickly dissipated after passing through the curved duct and the flow became well developed with a low turbulence level in the straight duct. The turbulence level in a duct system is also an important parameter to determine the location of the sampling section and minimize the turbulent fluctuations. For

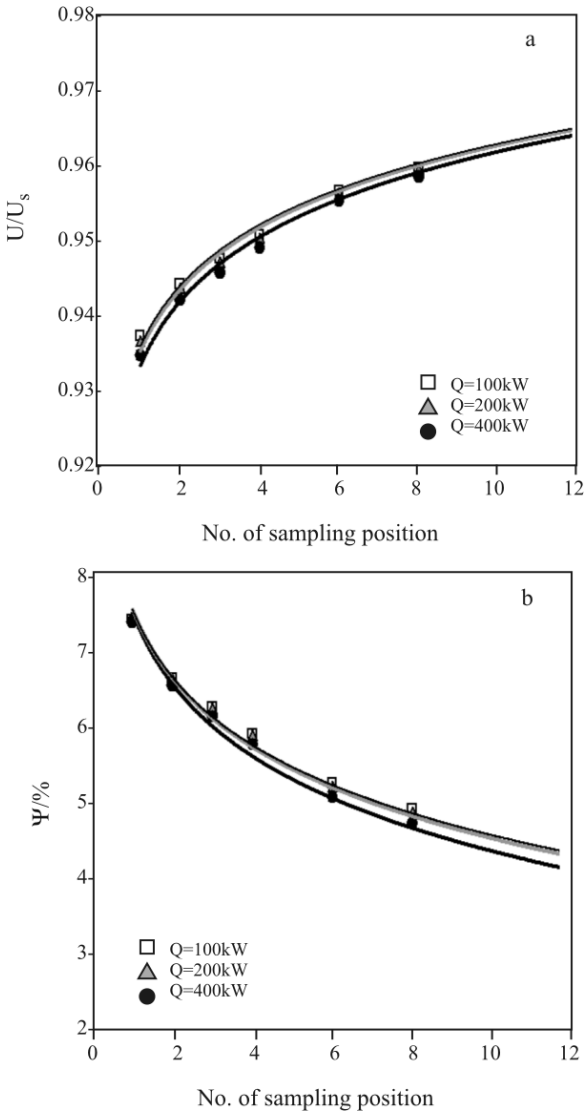

Fig. 7 The effect of the number of evenly-spaced sampling positions on the a – mean velocity ratio and the b – uncertainty of the heat release rate calculation

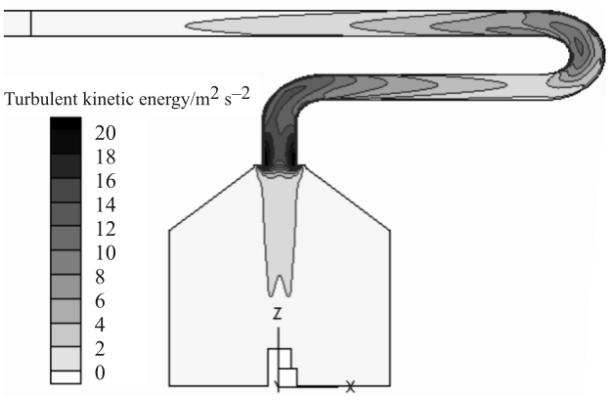

Fig. 8 The turbulent kinetic energy field for the case of a 200 kW fire

the duct system in this study, the turbulent kinetic energy of the location B is about 3 times higher than that of the location C.

Conclusions

The characteristics of the heat and mass flow inside the hood and duct system of a large scale oxygen consumption calorimeter were investigated using a CFD model with the volumetric heat and mass source model. The conclusions are summarized as follows:

- The CFD model used a simplified combustion sub-model to simulate the fire-driven flow with the explicit heat and mass sources assigned to the fire region. The model was validated using experimental measurements for the oxygen depletion factor and the gas temperature at the sampling position. The heat release rates for the CFD results were in good agreement with the measured heat release rate. The maximum difference was approximately 4% for the 400 kW fire.
- Temperature and species fields across the exhaust duct were relatively uniform compared to the velocity field. The flow field needs longer straight sections to reach the fully developed conditions. Unless there is insufficient length of straight duct, the representative velocity might have large uncertainty in the flow shape factor due to the limited number of sampling positions at each sampling section as well as the uncertainty of probe itself.
- The present study examined the effect of the number of sampling points across the duct on the averaged velocity and the percentage error of the measured heat release rate. As expected, the averaged velocity was close to the surface averaging velocity as the number of sampling positions increased. But, the sampling efficiency ($d(\overline{U}/\overline{U}_s)/dN$) decreased with increasing the number of sampling points (N). This information can be useful in the design of exhaust duct systems, especially if the effect of sampling position on the representative velocity is considered.

Accurate measurement of heat release rate using oxygen consumption calorimetry is challenging, requiring measurement of several quantities in real time. The uncertainty of the measured HRR not only depends on the probe itself, but also on the design of the exhaust duct system to obtain the representative quantities in the duct. This work contributes to an understanding of the flow characteristics inside an exhaust duct and illustrates how CFD can be used to design the performance of oxygen consumption calorimetry in fire testing.

Acknowledgements

The authors are grateful to Anthony Hamins, Alexander Maranghides, Laurean DeLauter and Marco Fernandez for helpful discussions and technical supports. Sung Chan Kim gratefully acknowledges support from a Korea Research Foundation Grant funded by the Korean Government (MOEHRD, Basic Research Promotion Fund) (KRF-2007-313-D00927).

References

1 Q. Xu, G. J. Griffin, Y. Jiang, A. D. Bicknell and G. P. Bradbury, J. Therm. Anal. Cal., online available.
2 Q. Xu, G. J. Griffin, Y. Jiang, C. Preston, A. D. Bicknell, G. P. Bradbury and N. White, J. Therm. Anal. Cal., 91 (2008) 355.
3 J. P. Redfern, J. Thermal. Anal., 35 (1989) 1861.
4 C. Huggett, Fire Mater., 4 (1980) 11.
5 R. A. Bryant, T. J. Ohlemiller, E. R. Johnsson, A. Hamins, B. S. Grove, W. F. Guthrie, A. Maranghides and G. W. Mulholland, NISTIR 7052, (2004).
6 W. J. Parker, NBSIR 81-2427-1(1982).
7 B. J. McCaffrey and G. Heskestad, Combust. Flame, 26 (1976) 125.
8 H., Xue, J. C. Ho and Y. M. Cheng, Fire Safety J., 36 (2001) 37.
9 A. J. Grandison, E. R. Galea and M. K. Patel, Univ. of Greenwich report for Fire Research and Development Group, (2001).
10 J. Wang, J. Hua, K. Kumar and S. Kumar, J. Fire Sci., 24 (2006) 393.
11 W. J. Parker, J. Fire Sci., 2 (1984) 380.
12 J. Ackeret, Elsevier Pub. Co., (1967) 1.
13 M. Rowe, J. Fluid Mech., 43 (1970) 771.
14 R. W. Yeager, J. Fire Sci., 4 (1986) 276.

Received: September 5, 2007
Accepted: March 18, 2008
OnlineFirst: June 25, 2008

DOI: 10.1007/s10973-007-8696-1